Fall November, 2006

Injection, trapping, and acceleration of electrons in a three-dimensional nonlinear laser wakefield

Serguei Y. Kalmykov
Leonid M. Gorbunov
Patrick Mora
Gennady Shvets

Injection, trapping, and acceleration of electrons in a three-dimensional nonlinear laser wakefield

S. Yu. Kalmykov[a)]
Department of Physics and Institute for Fusion Studies, The University of Texas at Austin, One University Station, C1500, Austin, Texas 78712

L. M. Gorbunov
P. N. Lebedev Physics Institute, Russian Academy of Sciences, Leninskii Prospect 53, Moscow 119991, Russia

P. Mora
Centre de Physique Théorique (UMR 7644 du CNRS), École Polytechnique, 91128 Palaiseau, France

G. Shvets
The Department of Physics and Institute for Fusion Studies, The University of Texas at Austin, One University Station, C1500, Austin, Texas 78712

(Received 7 July 2006; accepted 19 September 2006; published online 7 November 2006)

It is demonstrated that the accelerating and focusing phases of the nonlinear three-dimensional axisymmetric laser wake can almost entirely overlap starting from a certain distance behind the laser pulse in homogeneous plasma. Such field structure results from the curvature of phase fronts due to the radially inhomogeneous relativistic shift of plasma frequency. Consequently, the number of trapped low-energy electrons can be much greater than that predicted by the linear wake theory. This effect is favorable for quasimonoenergetic acceleration of a considerable charge (several hundreds of pC) to about 1 GeV per electron in the plasma wakefield driven by an ultrashort (~30 fs) weakly focused ($r_0 \sim 100$ μm) petawatt laser pulse. © *2006 American Institute of Physics*.
[DOI: 10.1063/1.2363172]

I. INTRODUCTION

Advances in laser engineering have recently enabled petawatt (PW) facilities delivering pulses shorter than 100 fs.[1,2] A laser of this class can be a key element of a compact electron accelerator [laser wakefield accelerator (LWFA), Ref. 3]. High-charge low-emittance ultrashort (tens of fs) electron bunches accelerated by the laser-driven plasma wakes can be used for radiotherapy in medicine, ultrafast radiolysis in chemistry,[4,5] fine structure imaging in biology and material science, and accelerator physics.[6] In the LWFA, one advantage of using an ultrashort (tens of fs) PW laser beam is operating under conditions of loose focusing (focal spot about hundred microns) yet in the mildly relativistic regime (intensity above 10^{18} W/cm^2). The excited weakly nonlinear three-dimensional (3D) electron plasma wave (EPW) does not break transversely[7] over many periods yet has the accelerating gradients of tens of GeV per meter. The diffraction limited laser-plasma interaction length of order 10 cm promises reaching GeV electron energy with unguided laser beam.[8] Avoiding strong relativistic self-focusing[9] in tenuous plasmas due to the short pulse duration[8,10] ensures stable operating conditions with considerable flexibility in parameters and good control over the properties of accelerated bunch(es).[6] All these features are favorable for the standard LWFA scheme[3] with external electron injection from state-of-art rf guns.[11–14] These injectors supply hundred-pC monoenergetic beams of few-MeV electrons; the beams have picosecond duration and can be focused down to 100 μm spots.[14] Thus, feasibility of the standard LWFA critically depends on the capability of the plasma wave to trap/accelerate a significant charge from an externally injected unbunched slow electron beam.[15]

For applications, low transverse emittance and few-percent final energy spread can be achieved by reducing the initial electron energy to the level of a few MeV.[8,15,16] In this case, however, linearized models of laser wakes in homogeneous plasmas predict an abrupt decline in the number of trapped electrons.[17] We show in this paper that such conflict is naturally resolved in the regimes of interest (similar to those considered in Refs. 6, 8, and 17). The relativistic nonlinearity of the 3D axisymmetric plasma wake does enable high (tens of percents) collection efficiency of a few-MeV electrons from long (above the period of plasma wave) and wide (of the order of laser spot size) electron beams.

In the nonlinear wake, accelerating and focusing phases overlap much stronger than in a linear wake in homogeneous plasmas. This is reminiscent of the plasma channel wakefield accelerators.[18] In the uniform background plasmas considered here, this phenomenon is entirely due to the radially varying relativistic frequency shift[7,8,19,20] responsible for the curvature of the constant phase surfaces (wave fronts). The curvature builds up progressively with the distance behind the driver;[7,19] consequently, the regions of radial focusing shift toward the accelerating regions, and the overlap between the focusing and accelerating phases (the accelerating-focusing phase, AFP) within each period exceeds the quarter-period given by the linear theory.[21] We show that even in the

[a)]Electronic mail: kalmykov@physics.utexas.edu

mildly relativistic regime the AFP extension can be significant already in the second wave bucket; as the distance behind the driving pulse grows, the AFP tends to the plasma half-period (the *full* accelerating phase becomes focusing). Hence, the collection efficiency of slow electrons from the initially long and wide injected beam appears to be greater more than twice against the linear estimates. The large radial and angular spread of injected electrons can now be tolerated, which considerably relaxes the requirements on the injector. Notably, the AFP extension in the *linear* wakes due to the radial profiling of the density in plasma channels[18] also results in the enhanced trapping of electrons from outer sources.[15,22]

The remainder of the paper is organized as follows: In Sec. II we investigate analytically and numerically the structure of accelerating and focusing forces in the mildly relativistic wake, and explain the origin of the AFP extension. In Sec. III, we prove that the wave nonlinearity boosts the efficiency of slow electron collection and support the simulation by the analytical estimates. In Sec. IV, we show the way to avoid the ponderomotive scattering of injected electron beam in vacuum in a realistic experimental setup. The conclusion summarizes the results and outlines directions of future work.

II. STRUCTURE OF ACCELERATING AND FOCUSING FORCES IN A 3D WEAKLY NONLINEAR PLASMA WAKE

In a 3D plasma wake excited by a localized axisymmetric source moving with a relativistic velocity and having the peak amplitude on axis (e.g., an ultrashort laser pulse[3] or electron beam[23]) all the physical quantities depend on the distance from the axis. Far from the axis the wake amplitude is small, and the density/potential perturbation is a linear sinusoidal harmonic with a period $\tau_p=2\pi/\omega_p$ (where $\omega_p=\sqrt{4\pi e^2 n_0/m_e}$ is the electron plasma frequency, $-|e|$ and m_e are the electron charge and rest mass). The wave amplitude grows toward the axis, and so does the relativistically corrected electron mass. Closer to the axis, the electron oscillations become anharmonic,[19,24] and their period increases leading to a finite curvature of the wave fronts. The radius of curvature drops as the distance behind the source of perturbation grows;[7,19] this effect admits direct experimental visualization via frequency-domain holography method.[25]

We shall find forces acting on an electron injected into the relativistic wakefield assuming that the driver is an ultrashort Gaussian laser pulse moving toward positive z (the wake driven by an electron beam can be considered in a similar fashion[20]). We introduce the following dimensionless variables: radius $r=k_p\sqrt{x^2+y^2}$, retarded time $\xi=\omega_p(t-z/v_g)$, and distance along the axis $z\equiv z/Z_R$. Here $k_p=\omega_p/c$ is the plasma wave number, $Z_R=(\pi/\lambda_0)R_0^2$ is the Rayleigh length of a laser beam with a wavelength λ_0 and focal spot radius R_0, and $v_g=c^2k_0/\omega_0\approx c$ is the group velocity of a laser with a frequency ω_0 and wave number $k_0=2\pi/\lambda_0$. At the instant $t=0$ the pulse center crosses the focal plane $z=0$. The normalized laser intensity in plasma is

$$|a(r,z,\xi)|^2=\mathcal{A}_0^2(z)e^{-2\xi^2/\xi_L^2-2r^2/\mathcal{R}_0^2(z)}, \tag{1}$$

where $\mathcal{A}_0=a_0/\sqrt{1+z^2}$ is a normalized peak vector potential at a given z [$a_0=0.85\times10^{-9}\sqrt{I(\mathrm{W/cm^2})}\lambda_0(\mu\mathrm{m})$, where I is the peak intensity in the focal spot], and $\mathcal{R}_0(z)=r_0\sqrt{1+z^2}$ is the local beam radius ($r_0=k_pR_0$ is the normalized focal spot size). The pulse is assumed short ($\xi_L\ll1$), wide ($r_0>2\pi$), and mildly relativistic ($a_0\gtrsim1$), hence it is immune to the relativistic self-focusing and propagates through a rarefied plasma in a vacuum-like fashion.[8,10] Perturbation of the electrostatic potential in the wake is proportional to the normalized laser intensity (1) and (normalized to $m_ec^2/|e|$) can be approximated as[8]

$$\phi(r,z,\xi>\xi_L)\approx\Phi(r,z)\sin[\Omega_p(r,z)\xi]. \tag{2}$$

Here, $\Phi(r,z)=\Phi_0(z)e^{-2r^2/\mathcal{R}_0^2(z)}$, $\Phi_0(z)=g(\xi_L)[\mathcal{A}_0^2(z)/2]^2$, and $g=\xi_L\sqrt{\pi/2}e^{-\xi_L^2/8}$. The relativistic frequency shift[24,26] $\Delta\omega_p(r,z)\equiv1-\Omega_p=3\Phi^2/16$ makes the wake phase transversely nonuniform. The pulse (1) is symmetric with respect to the center ($\xi=0$), so the wake behind it ($\xi>\xi_L$) does not acquire any additional radially inhomogeneous phase correction.[18] Equation (2) correctly describes features of almost electrostatic wide ($r_0>2\pi$) weakly nonlinear ($\Phi<1$) wake. Relativistic nonlinearity is dominating in this case, and the effect of self-consistently generated quasistatic magnetic fields[27] on injected electrons is negligible. The approximation used is cubic in Φ, but the potential anharmonicity is neglected. Only plasma frequency dependence on the amplitude is preserved. This approximation was explored by Noble[24] in the 1D limit, and we find it quite precise in the 3D axisymmetric case. From Eq. (2) we find normalized longitudinal ($F_z\equiv-\partial\phi/\partial\xi$) and radial ($F_r\equiv\partial\phi/\partial r$) forces[28] acting on a relativistic test electron,

$$F_z=-\Omega_p\Phi\cos(\Omega_p\xi), \tag{3a}$$

$$F_r=(\Phi'/\cos\Theta)\cos(\pi/2+\Theta-\Omega_p\xi), \tag{3b}$$

where $\Phi'=-r[2/\mathcal{R}_0(z)]^2\Phi(r,z)$, and the nonlinear phase shift of the radial force is

$$\Theta=\arctan(2\Delta\omega_p\xi)>0. \tag{4}$$

Inequalities $F_z>0$ and $F_r<0$ define the AFP and thus determine the volume of space useful for electron trapping and acceleration. In the linear wake ($\Theta\equiv0$), phase shift between F_r and F_z is $\pi/2$; hence, just a *quarter* of each period belongs to the AFP.[21] Relativistic phase (4) increases the overlap between accelerating and focusing phases; these almost merge at $\xi>(\Delta\omega_p)^{-1}$. Then $\Theta\approx\pi/2$, and the AFP extends to nearly a *half* wake period.

The weakly nonlinear Eqs. (3) and (4) are validated by 3D (in cylindrical geometry) particle-in-cell simulations via fully relativistic time-averaged code WAKE.[29] Slowly varying amplitude of a linearly polarized laser is computed in the extended paraxial approximation in the simulation box moving with a vacuum speed of light. The plasma response is quasistatic. The background plasma is fully ionized, homogeneous, and quiescent ahead of the pulse. The electron density is $n_0=1.68\times10^{17}$ cm^{-3}. In this section we numerically

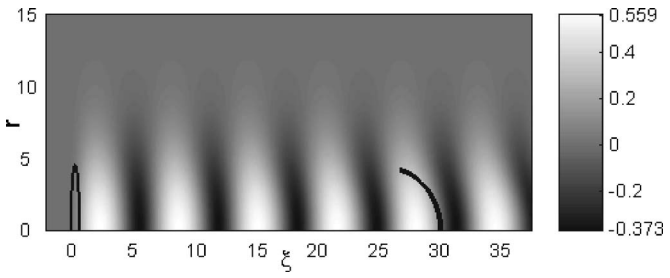

FIG. 1. Simulated normalized wake potential $\phi(r,z=0,\xi)$ behind the Gaussian pulse (1); contour near $\xi=0$—half-maximum of the laser intensity. Wave fronts are curved due to the radially nonuniform relativistic frequency shift. Radius of the arc crossing the axis at $\xi=30$ equals the radius of the wave front curvature $\rho(\psi=30)\approx 4.35$ from Eq. (5).

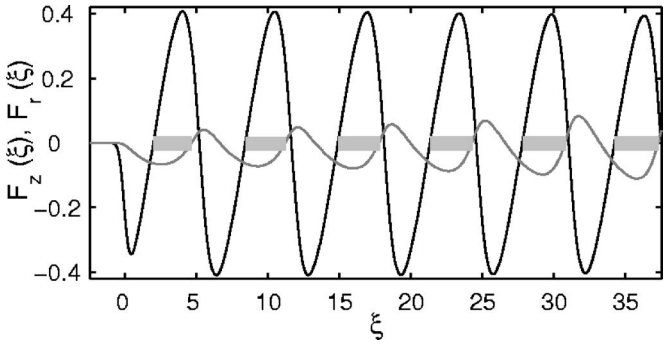

FIG. 2. Lineouts of simulated longitudinal $[F_z(\xi)$, black] and radial $[F_r(\xi)$, gray] forces acting on a test electron at $r=2$ in the vicinity of the laser focal plane $z=0$. The AFP intervals (where $F_z>0$ and $F_r<0$) are marked with light-gray rectangles. Gradually growing phase shift of the focusing phase toward the accelerating one extends the AFP to almost plasma half-period at $\xi\gtrsim 35$.

find the structure of the plasma wakefield excited by the Gaussian pulse (1) in the laser focal plane $z=0$ where the wake nonlinearity is the strongest. In the vicinity of $z=0$, the wake phase velocity $v_{\rm ph}\equiv c\beta_{\rm ph}$ is equal to the laser group velocity; hence the corresponding Lorentz factor is $\gamma_{\rm ph}=(1-\beta_{\rm ph}^2)^{-1/2}=\omega_0/\omega_{pe}$. The simulated wake is compared with the analytic approximation (2). We choose the normalized laser spot size and duration $r_0=7.84$ and $\xi_L\approx 0.586$ (in physical units, 100 μm and 25.5 fs, respectively). The laser wavelength is $\lambda_0=0.8$ μm (hence, $\gamma_{\rm ph}=102$), and $I=6.4\times 10^{18}$ W/cm^2 ($a_0=1.72$).

Figure 1 shows the potential structure at $z=0$. The wave fronts become visibly bent at $\xi>20$. From Eq. (2), the constant phase surfaces are given explicitly by the expression $[1-3\Phi_0^2(z)e^{-2r^2/\mathcal{R}_0^2(z)}]\xi=\psi$, where ψ is a positive constant. Given z and ψ, the normalized reciprocal radius of the wave front curvature on the axis is

$$\rho^{-1}(r=0,z,\psi)=(3\psi/2)[\Phi_0(z)/\mathcal{R}_0(z)]^2. \tag{5}$$

In the focal plane ($z=0$) and at a distance $\xi\approx\psi=30$ behind the pulse Eq. (5) gives $\rho\approx 4.35$ which agrees with the simulation. Extension of the AFP beyond the plasma quarter-period is observed very early: Eq. (4) predicts $\Theta\approx\pi/4$ already at the rear end of the second bucket, $\xi\approx 10$. For $\xi\approx 30$ and $r<r_0$, theory gives $\Theta\approx 2\pi/5$ which is also close to the numerical results. Longitudinal lineouts of the simulated forces (Fig. 2) demonstrate the AFP extension from roughly $3\pi/4$ at $\xi\approx 5$ to nearly π at $\xi\approx 35$. Simulated accelerating and focusing forces within the AFP are mapped out in Fig. 3; the forces are shown with a time delay $\sim 5\tau_p$ behind the driver. The approximate Eqs. (3) and (4) predict the AFP boundaries remarkably well, especially near ($r<2$) and far from the axis ($r>r_0$). When $r>r_0$, the wave is almost linear, and only a quarter-period belongs to the AFP; near axis ($r<2$), the AFP covers almost a half-period.

Nonlinearity of the focusing force (3b) shifts the peaks of F_r toward the axis and makes the radial force amplitude growing with the distance behind the pulse. Both effects are observed in simulation. The nonlinearity dominates in Eq. (3b) at $\Delta\omega_p\xi>1$, and the amplitude of radial force oscillations $\mathcal{F}_r\approx(3/8)\Phi'\Phi^2\xi$ grows with ξ linearly at a fixed distance from the axis. The maximum of $\mathcal{F}_r$ at a given ξ is achieved at $r_{\rm max}^{\rm nl}=r_0/(2\sqrt{3})$ [found from $\Phi''=-2(\Phi')^2/\Phi$]. This is different from the linear case in which the radial force maxima lay on the cylinder $r_{\rm max}^{\rm lin}=r_0/2$ (from $\Phi''=0$). Peaks of the simulated focusing force in Fig. 3(b) lie between $r_{\rm max}^{\rm nl}\approx 2.2$ and $r_{\rm max}^{\rm lin}\approx 3.9$.

To summarize, in the nonlinear 3D plasma wave the accelerating and focusing phases overlap almost entirely as the distance from the driver grows; in the mildly relativistic regime this takes just a few periods of plasma oscillations. Consequently, almost half of the plasma volume behind the driver becomes useful for the electron acceleration.

III. TRAPPING AND ACCELERATION OF EXTERNALLY INJECTED ELECTRON BEAM IN THE NONLINEAR WAVE

Throughout this section we assume that the laser pulse center crosses the focal plane at the instant $t=0$, and the test electron beam with a given length, angular spread, transverse size, and particle energy $\gamma_{e0}m_ec^2$ starts moving at some distance behind it [here, $\gamma_{e0}=(1-\beta_{e0}^2)^{-1/2}$ is the Lorentz factor, and $\beta_{e0}=v_{e0}/c$ is the normalized velocity of an electron]. In the plane of injection (laser focal plane) the test particles are uniformly distributed over a given wake period. Thus, they sample all the possible phases (accelerating, decelerating, focusing, and defocusing) of the structure. We shall formulate the criterion for electron trapping and acceleration in the 3D axisymmetric nonlinear wake. We shall also find theoreti-

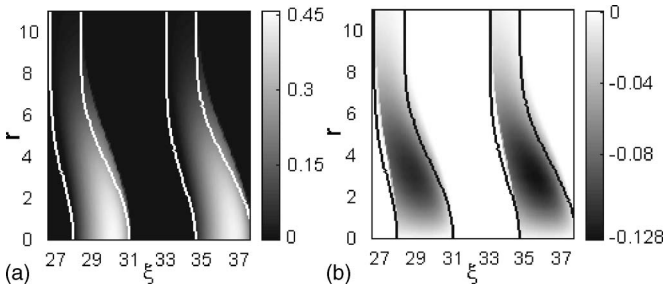

FIG. 3. Radial structure of (a) accelerating ($F_z>0$) and (b) focusing ($F_r<0$) forces inside the AFP in the laser focal plane $z=0$. The AFP borders (shown with black and white curves) are found analytically from Eqs. (3) and (4) and well coincide with the simulation result (gray scale).

cally the ratio of the accelerated charge to the charge injected [the collection efficiency (CE)] and use it for the explanation of numerical experiments.

A. Electron trapping in a 1D plasma wave

For consistency, we overview here the trapping process in the 1D geometry.[16,17,30–36] Through the remainder of the paper, the trapping is considered in the wake potential which varies between the limits $\phi_{\min}$ and $\phi_{\max}$ and is a given periodic function of ξ. The trapped electron is confined in the potential bucket where it was injected, while the free one performs infinite motion (never stops) in the wave frame. In the wave frame, a slow electron ($\gamma_{e0}<\gamma_{\rm ph}$) slips from the injection point $\xi=\xi_0$ toward the accelerating phase. In the accelerating phase it can synchronize with the wave [i.e., $\gamma_e(\xi_r)=\gamma_{\rm ph}$] in the turning point $\xi=\xi_r$. Existence of the turning point for a given ξ_0 and γ_{e0} is the criterion of trapping in 1D. Conservation of the test electron Hamiltonian[31] $H=\gamma_e(1-\beta_e\beta_{\rm ph})-\phi$ links the turning point ξ_r with the point of injection ξ_0 through $\phi(\xi_0)-\phi(\xi_r)=\gamma_{e0}(1-\beta_{e0}\beta_{\rm ph})-\gamma_{\rm ph}^{-1}$, which in the limit $\gamma_{e0(\rm ph)}\gg 1$ simplifies[17] as

$$\phi(\xi_0)-\phi(\xi_r)=A\equiv(\gamma_{\rm ph}-\gamma_{e0})^2/(2\gamma_{\rm ph}^2\gamma_{e0}). \tag{6}$$

(The assumption $\gamma_{e0}\gg 1$ remains reasonable even for $\gamma_{e0}=2$; then, at $\gamma_{\rm ph}\sim 100$, A is defined with a precision better than 10%.) Now we find the interval of initial positions $\xi_{0\rm tr}$ (the trapping phase) from which an electron with a given γ_{e0} may start and further remain confined in the potential bucket centered at its maximum $\xi=\xi_{\rm m}$. Electrons stay within a bucket if $\phi(\xi_r-\xi_m)\geqslant\phi_{\min}$. This inequality together with Eq. (6) define the trapping phase:

$$\phi(\xi_{0\rm tr}-\xi_m)\geqslant\phi_{\min}+A. \tag{7}$$

If $A>\phi_{\max}-\phi_{\min}=\Delta\phi$, Eq. (7) gives an empty phase interval. In such an instance the initial electron energy is below the trapping threshold. If the injection energy is low, $\gamma_{e0}\ll\gamma_{\rm ph}$, the 1D trapping threshold is $\gamma_{e0}^{\rm 1D}>1/(2\Delta\phi)$. The length of the trapping phase interval from Eq. (7) depends not only on the amplitude, but also on the shape of potential. The general nonlinear 1D case is discussed in Appendix A. For the weakly nonlinear wave we employ the potential (2) with neglected radial dependence. Then, within a period centered at $\xi_m=\Omega_{p0}^{-1}(2\pi m+\pi/2)$, $m=0,1,2,\ldots$ [where $\Omega_{p0}=1-3\Phi_0^2/16$, and $\phi(\xi_m)=\Phi_0$], the trapping phase from Eq. (7) is

$$|\xi_{0\rm tr}-\xi_m|\leqslant\Omega_{p0}^{-1}\arccos(-1+\Phi_0^{-1}A). \tag{8}$$

In the 3D geometry, Eq. (8) gives just a necessary condition of trapping because it ignores the radial forces acting on a test electron near the turning point. The next subsection shows that such a neglect cannot be justified in the regimes of our interest. Correction of the trapping phase due to the effect of radial forces is calculated in Sec. III C.

B. Transverse electron motion in the vicinity of turning point

Radial motion of electrons in a 3D wake potential was examined in Refs. 34, 35, and 37–40. In particular, the synchrotron radiation from plasma wakes[41] is associated with betatron oscillations of the trapped and accelerated electrons.

In the vicinity of the turning point longitudinal dynamics of the electron becomes slow in the wave frame. At this moment, the sign of $F_r(\xi\approx\xi_r)$ determines whether the particle is confined in the potential bucket (trapped in 3D) or radially expelled. We assume further that the electron energy is constant along the trajectory (or varying adiabatically), and the radial velocity is much smaller than the speed of light. Hence, a roughly constant longitudinal velocity v_{ez} determines the electron mass in the transverse motion. The latter is governed by the approximate differential equation (in physical units) $m_e\gamma_\parallel d^2r/dt^2=|e|\partial\varphi/\partial r$, where $\gamma_\parallel=[1-(v_{ez}/c)^2]^{-1/2}\gg 1$ (see, for instance, Ref. 38). In the normalized variables of Sec. II this equation reads

$$d^2r/dt^2=F_r/\gamma_\parallel, \tag{9}$$

where F_r can be found, e.g., from Eq. (3b). Equation (9) describes the electron radial motion near the turning point and, under assumption of nearly constant $\gamma_\parallel$ and neglected phase slippage, agrees with those derived in Refs. 34 and 35. We assume that the electron reaches the turning point with the radial offset Δr and velocity $dr/dt=\Delta v_r$. The initial value problem for Eq. (9) can be solved numerically. In its generic form it describes large-amplitude betatron oscillations of trapped electrons. For our current purposes we consider the electron motion near axis [$r<r_0/(2\sqrt{3})$] where $F_r\propto r$ and neglect the wake amplitude variation along z [then $\mathcal{R}_0(z)\approx r_0$ and $\mathcal{A}_0(z)\approx a_0$ in Eq. (3b)]. Linearized Eq. (9) reads

$$d^2r/dt^2+B^2(\xi_r)r=0, \tag{10}$$

where $B^2(\xi_r)=B_0^2\cos\psi(\xi_r)$, $B_0=(2/r_0)\sqrt{\Phi_0/(\gamma_\parallel\cos\Theta)}$, and $\psi(\xi_r)=\pi/2+\Theta(\xi_r)-\Omega_p\xi_r$. If $\Delta r\ll r_0$ and initial radial velocity is zero, the normalized radial offset varies in time as $r=\Delta r\cos(Bt)$. Whether the electron stays near axis or is radially expelled depends on the sign of $B^2(\xi_r)$ [hence, on the sign of $\cos\psi(\xi_r)$].

If ξ_r belongs to the focusing phase ($\cos\psi>0$), the electron oscillates around the axis with the period (in physical units) $\tau_\perp=\tau_{\perp0}\sqrt{\cos\Theta/\cos\psi}$ where $\tau_{\perp0}=\pi(R_0/c)\sqrt{\gamma_\parallel/\Phi_0}$. The scaling of $\tau_{\perp0}$ with $\gamma_\parallel$ and Φ_0 coincides with that from Refs. 39 and 40. Simulation parameters of Sec. II ($R_0=100$ μm, $\gamma_\parallel\approx\gamma_{\rm ph}=102$, $\Phi_0=0.56$) give $\tau_{\perp0}\approx 14$ ps (for comparison, Rayleigh time $\tau_R=Z_R/c\approx 130$ ps); the corresponding frequency is $\omega_{\perp0}=2\pi/\tau_{\perp0}=0.45$ THz.

From the defocusing region ($\cos\psi<0$) the electron is radially expelled: its distance from axis increases exponentially with the characteristic growth rate $\omega_{\perp0}$ (here we imply $|\cos\psi|/\cos\Theta\sim 1$). If the turning point lies so close to axis that the radial expulsion remains negligible during the acceleration stage, the electron can gain some energy. The electron stays in the wake ($r<r_0$) during a Rayleigh time τ_R (characteristic time of acceleration) only if the initial offset is as small as $\Delta r<2r_0\exp(-\omega_{\perp0}\tau_R)$. For the parameters of Sec.

II, $\omega_{\perp 0}\tau_R \approx 58.3$, and $\Delta r/r_0 < 10^{-25}$. Hence, in the regime of our interest, all the electrons with turning points in the defocusing region are side-scattered almost instantaneously and have no chance to gain a significant energy. Knowing that the defocusing region is unavailable for acceleration, we proceed with calculating the CE of the 3D axisymmetric wakefield (2).

C. Collection efficiency of mildly nonlinear 3D axisymmetric wakefield

We shall find the trapping phase for slow electrons ($\gamma_{e0} \ll \gamma_{\rm ph}$) in the 3D plasma wave using the following physical considerations. We assume that an electron is not radially deflected on passing from the injection (ξ_0) to the turning (ξ_r) point. To neglect the radial perturbation of the trajectory between these points we require that the electron starts moving parallel to the axis in the region where the transverse force is well below maximum [$r \ll r_0/(2\sqrt{3})$]. Slippage between a slow electron and the wake takes time (trapping time) $\omega_p \tau_{\rm tr} \approx |\xi_0 - \xi_r|/(1 - v_{e0}/v_{\rm ph})$, which implies that the electron moves almost ballistically before the turning point (see also the discussion in Ref. 22). Taking $\gamma_{e0}=2$ and knowing that the injection and turning points are separated by less than one plasma period we find that trapping takes roughly 1% of the Rayleigh time under the parameters of Sec. II. During the acceleration stage we allow for the electron transverse motion and assume that all the particles with turning points in the defocusing region are lost. Then, we apply the trapping condition (6) from the 1D theory additionally assuming that only those electrons are trapped whose turning phase is *both* accelerating *and* focusing. This approach was used in Ref. 17 where trapping in the 3D linear wave was considered.

We shall consider the wake potential in the vicinity of the focal plane $z=0$ where the nonlinearity is the highest. As in Sec. III A, we select a bucket centered at an on-axis maximum, $\xi=\xi_m$, where $\phi(r=0,\xi_m)=\Phi_0$. Initially, the electrons are homogeneously distributed over the wake period, $|\xi_0 - \xi_m| < \pi/\Omega_{p0}$; they sample all the phases of structure: accelerating and decelerating, focusing and defocusing. In this case, the standard definition of CE for the monochromatic injection equates the fraction of trapped and accelerated particles to the ratio of the trapping phase interval to the plasma wave period[15]

$$\eta \equiv \Delta_{\rm tr}/(2\pi). \tag{11}$$

Now we shall find the trapping phase interval as a function of initial electron energy.

In the wave frame, an electron with $\gamma_{e0} \ll \gamma_{\rm ph}$ slips from the point of injection, slows down, and can eventually stop in the acceleration phase. The turning point (if it exists), should belong to the focusing phase. Then, Eq. (6) links the injection and turning points through

$$\cos[\Omega_{p0}(\xi_0 - \xi_m)] - \cos[\Omega_{p0}(\xi_r - \xi_m)] = \Phi_0^{-1} A. \tag{12}$$

In the linear case ($\Omega_p \equiv 1$), the turning phase is focusing if $\xi_r - \xi_m < \pi/2$. The trapping phase interval is then given by $|\xi_{0\rm tr} - \xi_m| \geqslant \arccos(\Phi_0^{-1}A)$ (Ref. 17), and its length is

$$\Delta_{\rm tr}^{\rm lin} = 2\arccos(\Phi_0^{-1}A). \tag{13}$$

Substitution of $\gamma_{e0}=2$, $\gamma_{\rm ph}=102$, and $\Phi_0=0.56$ gives $\Delta_{\rm tr}^{\rm lin} \approx 2.255 < \pi$. From Eq. (11), $\eta_{\rm lin} \approx 36\%$ of electrons are trapped.

Relativistic nonlinearity increases the overlap between accelerating and focusing phases: it shifts the boundary of focusing phase toward the potential minimum [the phase shift is given by Eq. (4)]. Electron remains in the focusing phase (hence, trapped in 3D) if the turning point satisfies the condition $\xi_r - \xi_m \leqslant \pi/2 + \Theta(\xi_r)$ (instead of $\pi/2$ in the linear case). Then, the inequality $\cos[\Omega_{p0}(\xi_{0\rm tr} - \xi_m)] \geqslant \Phi_0^{-1}A - \sin\Theta(\xi_r)$ following from Eq. (12) gives the trapping phase interval

$$\Delta_{\rm tr}^{\rm nl} = (2/\Omega_{p0})\arccos[\Phi_0^{-1}A - \sin\Theta(\xi_r)]. \tag{14}$$

An increase of $\Delta_{\rm tr}^{\rm nl}$ against the linear case is almost twofold: for $\Theta(\xi_r \approx 30) = 2\pi/5$, $\Delta_{\rm tr}^{\rm nl} \approx 4.51$. The resulting increase in the CE, $\eta_{\rm nl} \approx 72\%$ (against $\eta_{\rm lin} \approx 36\%$) is confirmed by the subsequent simulations.

The simulation parameters of laser and plasma are specified in Sec. II. We trace the evolution of physical quantities from the laser focal plane $z=0$ to the extraction plane $z_{\rm ext}=2$ (propagation length ≈ 8 cm). The boundary condition for radiation at $z=0$ is given by Eq. (1). The laser power (1 PW) exceeds $P_{\rm cr}$ by a factor of 6. Variation of the peak intensity along the laser path in plasma (not shown here) is very similar to that in Fig. 6 at $z>0$. The laser does not self-focus and remains almost Gaussian (1) over the entire propagation length. We inject electrons in the laser focal spot where the wake nonlinearity is maximal (the potential structure in the plane of injection is shown in Fig. 1). Details of the electron acceleration procedure in the code WAKE are explained in Ref. 28 (see also Ref. 37). The electron radial distribution in the plane $z=0$ is Gaussian with the root-mean-square (rms) radius σ_e (in units k_p^{-1}) and rms angular spread α_e. The beam can propagate either coaxially or at an angle α_1 with the laser pulse.[37] The beam axis lies in the plane of laser polarization. In this section, $\alpha_e = \alpha_1 = 0$. To verify the theoretical estimates of the CE we take a narrow electron beam with the initial radius $\sigma_e = r_0/(2\sqrt{3}) \approx 2.2$ (in physical units, 30 μm). Monoenergetic electrons with the Lorentz factor $\gamma_{e0}=2$ are uniformly distributed in time over the wake period centered at $\xi_m \approx 28$ (nearly one half of this period belongs to the AFP). To evaluate the contribution from the plasma wave nonlinearity we made a complementary simulation with the same electron beam accelerated in the linearized wakefield [Eq. (2) with $\Delta\omega_p \equiv 0$] driven by the prescribed Gaussian pulse (1) with the peak amplitude $a_0=1.72$.

Figure 4(a) shows the final energy versus injection phase for the electrons accelerated in the fully nonlinear (black) and linearized Gaussian wake (red). Populations of accelerated electrons lie almost entirely within the limits (shown by arrows) theoretically predicted from Eqs. (13) and (14). Figure 4(b) shows the electron energy spectra. The number of electrons accelerated in the nonlinear wave to $\gamma > 900$ is $\eta_{\rm nl} \approx 67\%$. The CE of the linear wake is almost twice lower, $\eta_{\rm lin} \approx 32\%$. So, theoretically predicted ratio of the collection efficiencies (≈ 0.5) is well confirmed. A sharp peak in the

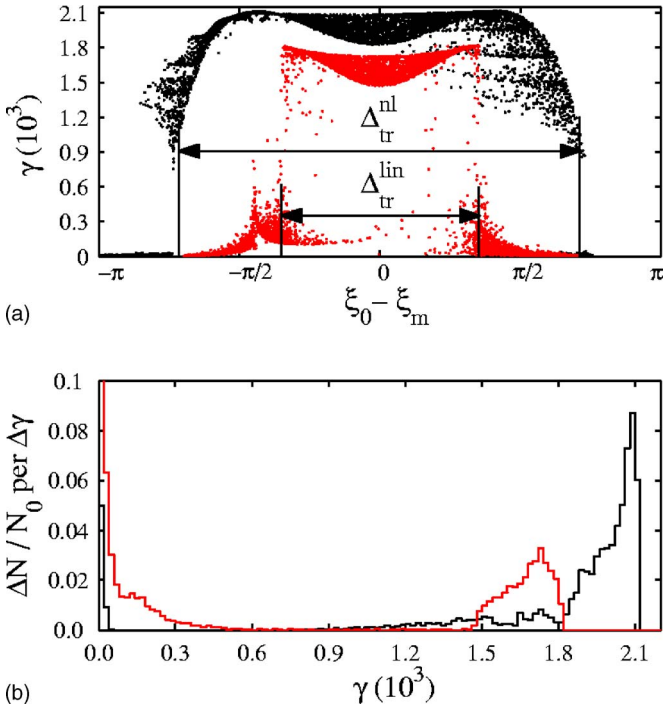

FIG. 4. (Color online) Energy of test electrons crossing the extraction plane $z_{ext}=2$. $N_0=10^4$ electrons with $\gamma_{e0}=2$ were injected in the fifth period ($\xi_m=28$) of the linear (red) and nonlinear (black) wake in the laser focal spot. (a) Energy vs injection phase. The analytically calculated boundaries of the trapping phase are shown. (b) The number of accelerated electrons per bin of the energy spectrometer (the bin size $\Delta\gamma=20$).

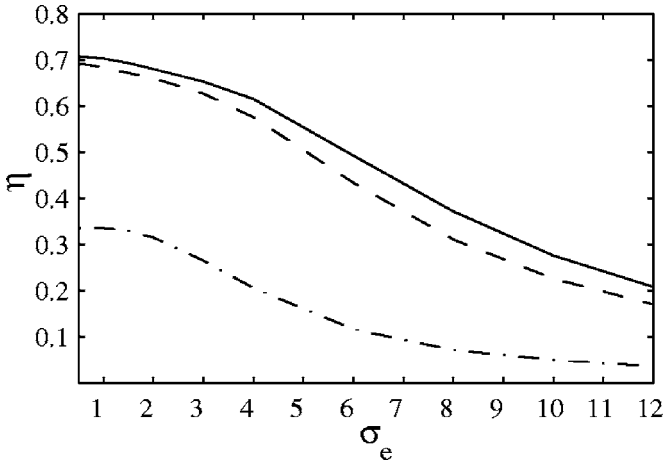

FIG. 5. Collection efficiency of the second (dashed line) and fifth (solid line) periods of the nonlinear wake as a function of the beam radius at the injection plane. The dashed-dotted line shows the CE for an arbitrary period of a linearized wake. Number of injected electrons $N_0=10^4$ and initial gamma factor $\gamma_{e0}=2$ are fixed. Laser waist radius is $r_0=7.84$.

spectrum of electrons accelerated in the nonlinear wake [4.75% spread at half-maximum around $\gamma_{max}=2100$ (energy, ~1.07 GeV)] contains roughly 35% of injected electrons. The low-energy tail extended from $\gamma=900$ to 1800 contains about 10% of injected electrons. It forms in the course of wakefield evolution along the acceleration length. As the laser diverges in the plasma, the wake amplitude drops, and the AFP shrinks. Hence, some of the initially trapped electrons are transversely expelled from the bucket and their acceleration ceases. This effect becomes noticeable only within the second half of acceleration length, $z \geqslant 1.25$.

Quasi-1D analytical estimates of the CE appear quite precise in the case of narrow electron beams ($\sigma_e < r_0$). Yet, we have no analytic theory for electron trapping from the wide beams ($\sigma_e \sim r_0$) injected into 3D potential wells of complicated configuration. In this case we extract the CE from the simulation data. We made several runs with all the parameters the same as of Fig. 4, except for the beam initial radius which we varied from 0.5 to 12 (roughly 160 μm). In the nonlinear simulation, the electrons were injected in the second ($\xi_m \approx 8.35$) and fifth ($\xi_m \approx 28$) periods. The CE from the numerical experiment is plotted as a function of σ_e in Fig. 5. The number of electrons trapped in the nonlinear wake decreases very steadily from roughly 70% to 20%. On the contrary, the CE of the linear wake drops abruptly from initial 35% to roughly 3.5%. Physically, the nonlinear increase of the focusing force preserves reasonably high trapped charge (tens of percents) even when the beam at the injection plane is wider than the laser waist. Technically difficult focusing of an injected high-charge slow electron beam into a sub-100 μm spot[17] is thus not necessary. [An observation of effective trapping of weakly relativistic electrons ($\gamma \sim 1$) on the periphery of nonlinear wake ($r \gtrsim r_0$) was made earlier in Ref. 34 (without emphasis on enhanced collection efficiency).]

In conclusion, the optimal for trapping and acceleration experimental strategy involves laser focusing on the edge of the plasma and the electron beam injection in the laser focal spot (where the wake is maximally nonlinear). This approach helps achieve quasimonoenergetic acceleration of maximal charge to ~1 GeV per electron with an external injection from conventional sources. Nonlinear corrections to the radial focusing force extend the volume of space available for particle trapping and acceleration. Therefore, the CE in the described regime exceeds more than twice that expected from linear theory. Collection of injected slow electrons can be highly efficient (tens of percents) even in the case of weakly focused (wider than laser waist) electron beam. Thus the requirement on tight beam focusing in the laboratory experiment[17] is relaxed.

IV. ELECTRON BEAM INJECTION: FROM VACUUM INTO THE PLASMA

We assumed so far that the unperturbed beam of low-energy test electrons starts moving in the wake of the laser pulse. Practical implementation, however, requires more careful consideration of the injection process. In practice, interaction between the laser pulse and slow electron beam begins not in the plasma (through the wake) but yet in vacuum.[42] The pulse outruns slow electrons before the plasma entrance, and its relativistic ponderomotive force perturbs their trajectories. In particular, the ponderomotive force of a relativistically strong pulse ($a_0 > 1$) scatters a few-MeV electrons in the direction of the intensity gradient. The ponderomotive scattering (PS) is independent of the direction of laser polarization.[42] The PS can preclude injection of the

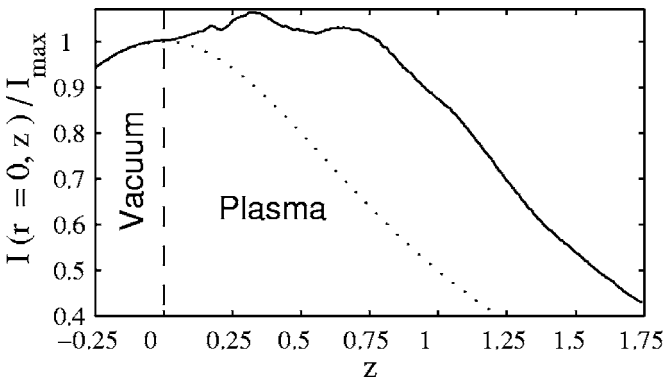

FIG. 6. The peak laser intensity normalized to $I_{max}=6.4\times10^{18}$ W/cm^2 vs propagation distance. Laser evolution is traced from the point of contact in vacuum $z_c=-0.25$. Solid line—propagation through the plasma slab of density $n_0(z>0)=1.68\times10^{17}$ cm^{-3} $(P=6P_{cr})$; dotted line—propagation in vacuum.

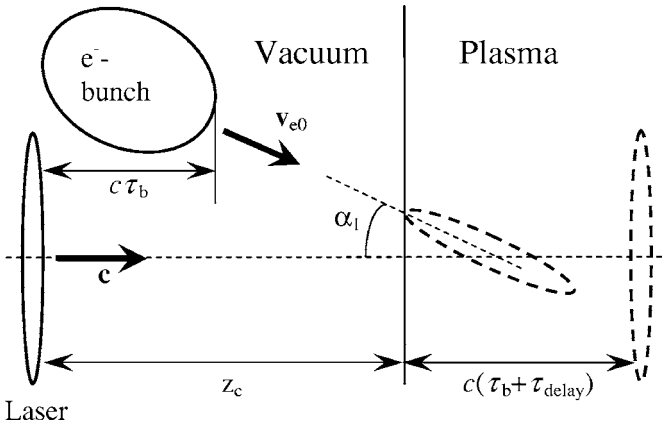

FIG. 8. In-plane schematic of the electron injection (true spatial scales are not preserved). To avoid the ponderomotive scattering by the overtaking laser pulse yet in vacuum, the slow electron beam (with small angular divergence $\alpha_e\leqslant1°$) is injected at a small angle α_1 (about 1°) with respect to the axis. The body of the beam thus remains unperturbed. The beam arrives in the plasma behind the laser pulse with a given time delay (τ_{delay}) which is chosen so as to make the electrons trapped in the desired wake potential bucket(s).

majority of beam electrons into the wake thus reducing CE and deteriorating the final quality of the accelerated bunch(es). In this section we explore one opportunity to bypass this potential difficulty.

PS is the most adverse in the case of coaxial injection (electron beam moving collinearly with the laser pulse). We show this in the numerical experiment with the electron beam parameters typical of state-of-the-art injectors:[4,11] $\gamma_{e0}=4$ (1.6 MeV), $\tau_b=810$ fs, $\alpha_e\approx0.5°$, rms radius at the plasma border 72 μm (the transverse normalized emittance $\gamma_{e0}\epsilon_\perp\approx0.8\pi$ mm mrad, where $\epsilon_\perp$ is the geometric rms emittance[37]). Average beam velocity is directed along the laser axis ($\alpha_1=0$). The number of test electrons is 3×10^4. The laser with the parameters from Sec. II focuses on the edge ($z=0$) of a neutral helium slab; the gas slab extends to $z_{ext}=1.75$ (7 cm) and has 0.5 mm linear density ramps on either side. Tunnelling ionization produces a flat-top plasma column with background electron density $n_0=1.68\times10^{17}$ cm^{-3} (then, $\tau_b\approx3\tau_p$, and $\sigma_e=5.5$). The head of electron beam arrives in plasma behind the pulse with a delay $\tau_{delay}\approx0.5\tau_p\approx135$ fs. Simulation starts in vacuum at the point of contact $z_c=-0.25$ (about 1 cm from the plasma boundary) with the laser pulse situated immediately behind the electron beam. The position of the point of contact is found from $|z_c|\approx[\beta_{e0}/(1-\beta_{e0})](L/Z_R)$ where $L=c(\tau_L+\tau_b+\tau_{delay})$.

Figure 6 shows that the relativistic self-focusing in plasma is almost avoided (the peak intensity increases against that in the focal plane by less than 7%). The relativistic nonlinearity, however, is slightly decompensated,[8] and the laser pulse does not diverge over almost one Rayleigh length. This helps to increase final electron energy.

Figure 7 demonstrates poor trapping efficiency in the case of coaxial injection. The electron beam is completely ruined at the injection plane $z=0$: the majority of electrons is side-scattered, and only 3.5% of injected particles are trapped (in four consecutive periods).

To reduce the effect of PS we propose to inject the beam obliquely at an angle α_1 (Fig. 8). This can be naturally realized in the laboratory. Only the edge of the electron beam is then exposed to the laser ponderomotive force; the beam body arrives in plasma almost unperturbed. On the other hand, the transverse focusing force of the wide nonlinear wakefield is strong enough to trap a significant amount of obliquely injected electrons. Simulation results shown in Figs. 9 and 10 testify that 45.2% of particles injected at an angle $\alpha_1=1.5°$ are trapped: 5%, 16.2%, 21.5%, and 2.5% of electrons end up the second, third, fourth, and fifth wake

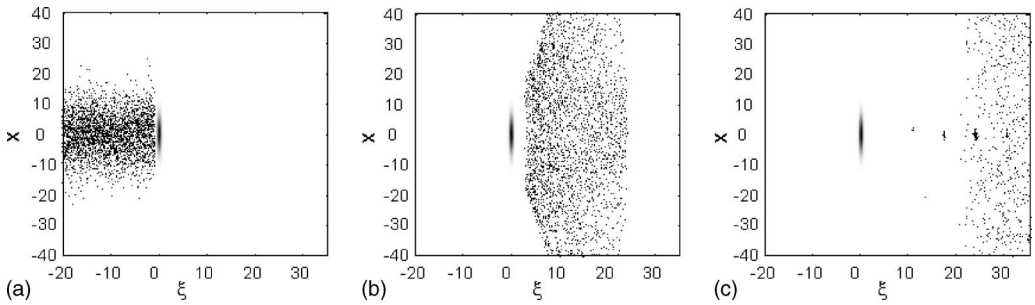

FIG. 7. Ponderomotive scattering in the case of coaxial injection. Laser intensity (gray scale at $\xi\approx0$) and electron positions in the $\xi-x$ plane (plane of laser polarization) are shown in the window moving with a speed of light at (a) point of contact $z_c=-0.25$, (b) injection point $z=0$, and (c) inside plasma, $z=0.25$. Almost all the injected electrons are side-scattered; only 3.5% reach the region near the axis and become trapped.

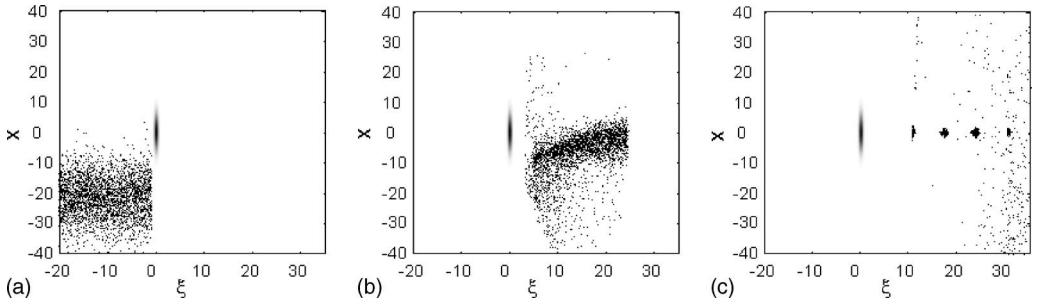

FIG. 9. Ponderomotive scattering in the case of oblique injection ($\alpha_1=1.5°$; other parameters are the same as in Fig. 7). Quantities shown are the same as in Fig. 7. The detrimental effect of PS is relaxed: about 45.2% of injected electrons are trapped in the four wake periods.

periods, respectively. The quasimonoenergetic acceleration follows. The electron energy spectrum shown in Fig. 10(a) exhibits the peak at $\gamma=2060$ with 8% spread. 29% of injected electrons gain energy above $\gamma=1950$ (≈ 1 GeV). The electrons are trapped in four periods, so the accelerated bunches come out of the plasma with a periodicity $1/\tau_p \approx 3.7$ THz. Each of them has a duration less than 45 fs. If the beam were initially shorter ($\tau_b=270$ fs $\approx \tau_p$), electrons could be accelerated as a single bunch.

The transverse coordinate and momentum space of electrons with $\gamma>1950$ is shown in Figs. 11(c) and 11(d), respectively. The radial wake focuses the bunches so tightly that the initial asymmetry of injection has almost negligible effect on the final beam spot in both coordinate and momentum space. The mean radius of accelerated bunches is about 15 μm, and the angular spread is about 1.3 mrad. Emittance of electrons from the energy peak is $\gamma\epsilon_\perp \approx 17\pi$ mm mrad; this value is preserved with the accuracy $\pm 10\%$ along the entire acceleration length (except in the proximity of plasma boundary). The oblique injection produces a 20% emittance dilution; a test simulation of the coaxial injection (same as Fig. 7) with the ponderomotive force turned off in the equations of motion of test particles gives $\gamma\epsilon_\perp \approx 14.5\pi$ mm mrad. The defocusing effect of plasma wakes excited on the density ramps is negligible in this regime (we find this by repeating the above simulations in the uniform preformed plasmas).

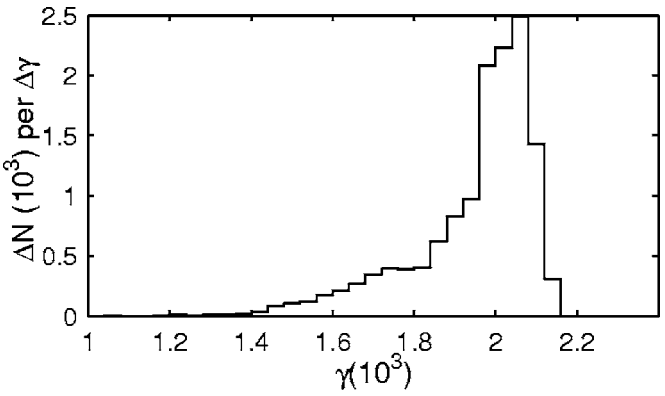

FIG. 10. Number of accelerated electrons per energy spectrometer bin (the bin size $\Delta\gamma=40$) at $z_{ext}=1.75$. Electrons are collected from all four periods where they were trapped (Fig. 9). Total number of injected particles is 3×10^4.

The sharp (almost 20-fold) increase in emittance during the trapping stage ($0<z<0.05Z_R$) can be explained mainly due to the strong nonadiabaticity of electrons which are not only focused but also longitudinally accelerated; they become synchronous with the wave, i.e., gain more than 10 times the initial energy, within less than a half betatron period. Additionally, almost 85% of electrons initially experience strongly nonlinear focusing force [they are injected with radial offsets $>r_0/(2\sqrt{3})$]. The emittance growth in the case of wide and slow injected electron beams was discussed earlier in Refs. 32 and 39. Our simulations reveal less emittance growth of an obliquely injected narrow beam ($\sigma_e \sim 1$); in this case, however, the spot asymmetry of the accelerated bunch(es) becomes rather pronounced.

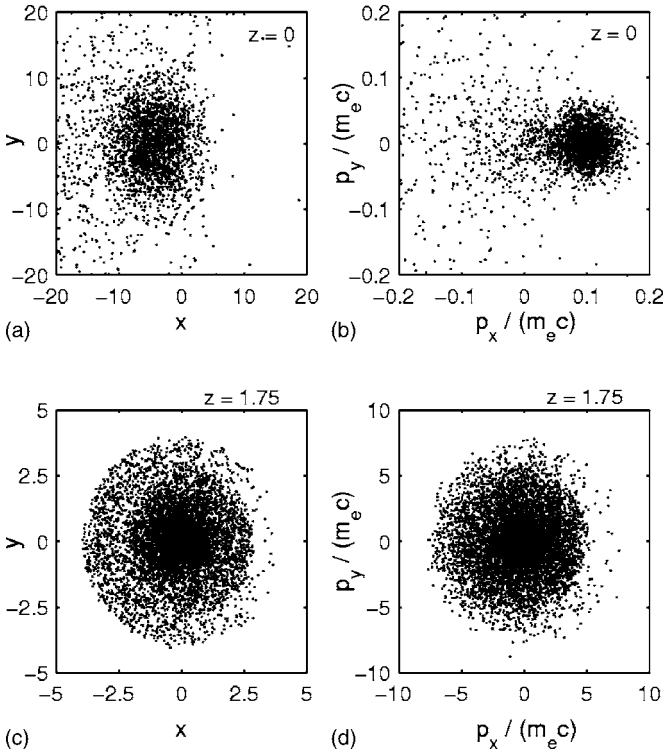

FIG. 11. Transverse coordinate [(a), (c)] and momentum [(b), (d)] space of the electron beam. At the plasma entrance $z=0$ [plots (a) and (b)] every tenth particle is shown. At the extraction point, $z_{ext}=1.75$ [plots (c) and (d)] only electrons with $\gamma>1950$ are presented. Despite asymmetric injection, the output beam reveals quite a good symmetry in both coordinate (with some aberrations) and momentum space.

In the realistic situation, total accelerated charge is limited by the 3D beam loading. Taking the final spot size of the bunch and knowing that the peak normalized electric field of the wake at the extraction plane is $E_{\max}(z_{\text{ext}}) \approx 0.25$ (in the units $m_e\omega_p c/|e|$), we get from Eq. (19) of Ref. 22 the upper limit on the number of accelerated electrons per wake bucket: $N_{\text{acc}} < 8.6\times 10^8$ (which corresponds to the charge $Q_{\text{acc}} < 0.14$ nC). Injecting into several wake buckets can help raise the charge to 1 nC with the beam loading still negligible. Capability of the system to trap and quasimonoenergetically accelerate a significant charge is favorable for its application as an element of a multistage high-energy laser-based linac.[40] However, strong radial wakefield preserves the bunch emittance almost an order of magnitude higher than the less demanding schemes can tolerate (e.g., SLC-type emittances are ~5 mm mrad[43]). Any measure taken for emittance reduction (either tighter focusing of the incoming few-MeV electron beam, perhaps, to a micron-size spot,[44] or subsequent cooling of GeV electrons[45]) is associated with severe charge losses. But even under the hostile conditions of tradeoff between the accelerated beam quality and net accelerated charge, the excellent collecting capability of the weakly nonlinear wake helps save charge and preserve the efficiency of the accelerating unit.

V. CONCLUSION

We have shown that a PW laser based LWFA can be optimized to achieve 1 GeV electron energy with a few-percent energy spread, moderate angular spread, and high charge (>100 pC per shot). The accelerating unit can consist of two stages. For the first stage a state-of-the-art rf gun[11] can be employed which supplies hundreds of pC electron beams of sub-ps duration for injection into the 3D axisymmetric weakly relativistic wake driven in a homogeneous plasma ($n_0 \sim 10^{17}$ cm^{-3}) by an ultrashort (~30 fs) weakly focused ($R_0 \sim 100$ μm) PW laser. The nonlinear laser wakefield in the vicinity of focal spot can collect in a few tens of percent of the injected charge from the slow (~1 MeV) unbunched electron beam with the radius exceeding the laser spot size. High collection efficiency is due to the increased overlap between focusing and accelerating phases produced by the radially inhomogeneous relativistic frequency shift. We have seen that the GeV electrons have some angular and, hence, transverse momentum, spread. This implies observable radiation emission due to the betatron oscillations of trapped electrons. Therefore, plasma wake accelerating externally injected electrons could be used as a source of synchrotron radiation. Also, moving beyond the simplistic estimates of the beam loading may become necessary for practical applications. These are the directions of future work.

ACKNOWLEDGMENTS

S.Yu.K. thanks C. Clayton, R. Hubbard, V. Malka, C. Sears, and M. Uesaka for discussions of various schemes of electron injection in the LWFA during the 2006 AAC Workshop.

This work was partly supported by CNRS (France) in the frame of cooperation with the Russian Academy of Sciences, by the U. S. Department of Energy under Contracts No. DE-FG02-04ER54763 and No. DE-FG02-04ER41321, and by the NSF Grant No. PHY-0114336 administered by the FOCUS Center at the University of Michigan, Ann Arbor.

APPENDIX A: ELECTRON TRAPPING IN THE FULLY NONLINEAR 1D ELECTRON PLASMA WAVE

Nonlinear modification of the wake potential profile near axis can increase the trapping phase interval. This purely 1D effect is independent of distance from the driver. The normalized 1D wake potential behind the driver ($\xi \gg \xi_L$) is described by Refs. 24, 31, 33, 46, and 47 $\partial^2\Psi/\partial\xi^2 + (1-\Psi^{-2})/2 = 0$. The weakly nonlinear limit follows from it at $\Psi = 1+\phi$, $|\phi| \ll 1$. If the potential reaches maximum $\Psi_{\max} = b$ at $\xi = \xi_{\text{m}}$, then

$$\xi - \xi_{\text{m}} = \pm \int_b^{\Psi} \frac{\sqrt{x}dx}{\sqrt{(b-x)(x-b^{-1})}} = \mp 2\sqrt{b}E(\mu,\kappa), \quad \text{(A1)}$$

where $\mu = \arcsin\sqrt{(b-\Psi)/(b-b^{-1})}$, $\kappa = \sqrt{1-b^{-2}}$, and $E(\mu,\kappa)$ is the elliptic integral of the second kind.[48] The wave period is $\tau_{\text{nl}} = 4\sqrt{b}E(\pi/2,\kappa)$, where $E(\pi/2,\kappa)$ is the complete elliptic integral. The ultrarelativistic limit of Eq. (A1) is obtained at $\kappa \sim 1$ (or $b \gg 1$). Then, $E \approx (2/\pi)\ln[\tan(\mu/2+\pi/4)]$, and, as a result,

$$\Psi = b\left\{1 - (1-b^{-2})\cos^2\left[2\arctan\exp\left(\frac{\pi(\xi-\xi_{\text{m}})}{4\sqrt{b}}\right)\right]\right\}.$$

By analogy with this formula, we express the generic wake potential as $\Psi = bf(\xi-\xi_{\text{m}},b)$, where $b^{-2} \leqslant f \leqslant 1$. The form-factor f may be calculated from Eq. (A1) numerically.

Let us assume that an electron with the gamma factor γ_{e0} is injected in the interval $\xi_{\text{m}} - \tau_{\text{nl}}/2 \leqslant \xi_0 \leqslant \xi_m + \tau_{\text{nl}}/2$. The electron stops in the wave frame at the turning point $\xi = \xi_r$, where $\gamma_e(\xi_r) = \gamma_{\text{ph}}$. In the limit $\gamma_{e0(\text{ph})} \gg 1$, conservation of the test electron Hamiltonian gives [compare with Eq. (6)] $f(\xi_0 - \xi_m) - f(\xi_r - \xi_m) = b^{-1}A$. The electron is trapped in the 1D wake potential if the turning point is within the same plasma period, that is, $f(\xi_r - \xi_m) \geqslant b^{-2}$. Given b, the corresponding interval of the initial electron positions (trapping phase) can be retrieved numerically from

$$f(\xi_{0\text{tr}} - \xi_m) \geqslant b^{-2} + b^{-1}A. \quad \text{(A2)}$$

Let us compare the trapping phase interval following from a fully nonlinear theory [Eq. (A2)] with that inferred from a sinusoidal approximation [Eq. (8)] for the parameters of potential structure mapped out in Fig. 1 ($\gamma_{\text{ph}} = 102$, $b = 1.56$) and $\gamma_{e0} = 2$. The length of the trapping phase interval from exact nonlinear Eq. (A2) is $\Delta_{1\text{D}}^{\text{nl}} \approx 5.3$. The linear approximation (8) gives the shorter range of the trapping phases, $\Delta_{1\text{D}}^{\text{lin}} \approx 4.35$. Hence, even in the mildly relativistic case ($b < 2$) the 1D wake anharmonicity broadens the trapping phase interval. However, in the realistic 3D geometry the effect of radial (defocusing) forces reduces the length of the trapping phase (from Sec. III C, $\Delta_{\text{tr}}^{\text{nl}} \approx 4.5$ and

$\Delta_{tr}^{lin} \approx 2.26$). In the regimes considered in this paper the trapping phase is determined predominantly by the 3D relativistic effects.

APPENDIX B: BRIEF SUMMARY OF EXISTING SCHEMES OF ELECTRON INJECTION IN THE LWFA

There has been experimental progress[49] in the all-optical injection using colliding laser pulses.[50] Ponderomotive force of the large-amplitude driving pulse and the counterpropagating small-amplitude one pushes some plasma electrons strongly enough to make them trapped in the *first* period of the plasma wake (immediately behind the driving pulse). The scheme appears stable in the lab experiment[49] providing up to 10 pC of accelerated charge (with few percent energy spread) in every shot. Remarkable stability of the scheme is due to the fact that the trapped charge is far below the beam loading threshold, and the plasma wave is not broken under the experimental conditions.[49] However, the electrons can be injected in one wave bucket only; and manipulating the relative power of colliding pulses was so far insufficient to raise the accelerated charge above 10 pC.[49]

The other opportunity (the only one which has been so far feasible in the LWFA experiments) is the electron self-injection due to the radial plasma wave breaking.[51] The order of magnitude larger amount of trapped and accelerated charge (hundreds of pC, which is limited from above by the beam loading) could be virtually convenient for staged acceleration. Quasimonoenergetic acceleration was also achieved. However, the self-injection is also limited basically to just one wake period (the first one) and, what is more important, the amount of accelerated charge is poorly reproduced from shot to shot. And the accelerated bunch of self-injected electrons usually shows too large transverse emittance and poor pointing stability in the laboratory experiment. Substantial improvement of the stability can be achieved by introducing a multi-cm plasma channel (Ref. 52). However, if shot-to-shot stable acceleration of hundred pC charge without channeling is concerned (possibly in several consecutive wave buckets), more conventional rf injector technology[12,13] is not to be overlooked.

Coupling slow electron beams of considerable charge into small-scale structures and sub-ps synchronization time scales are common for many fields including, for instance, direct laser acceleration[44] and x-ray generation via inverse Compton scattering.[14] The state-of-the-art technology allows for the slow ($\sim$10 MeV) picosecond hundred-pC electron beams focusing down and coupling into structures of few tens of microns in radius.[14] The radial wake size in the regimes of our interest is an order of magnitude larger, hence requirements on the focusing systems can be relaxed. This makes an rf based electron injector[11] viable for LWFA applications.

[1] M. Aoyama, K. Yamakawa, Y. Akahane, J. Ma, N. Inoue, H. Ueda, and H. Kiriyama, Opt. Lett. **28**, 1594 (2003); see also Science **301**, 154 (2003).
[2] G. A. Mourou, T. Tajima, and S. V. Bulanov, Rev. Mod. Phys. **78**, 309 (2006).
[3] T. Tajima and J. M. Dawson, Phys. Rev. Lett. **43**, 267 (1979).
[4] A. Ogata, K. Nakajima, and N. Andreev, J. Nucl. Mater. **248**, 392 (1997).
[5] V. Malka, J. Faure, Y. Glinec, and Y.-A. Gauduel, L'Actualité Chimique **292**, 18 (2005) (in French).
[6] V. Malka, J. Faure, Y. Glinec, and A. F. Lifschitz, Plasma Phys. Controlled Fusion **47**, B481 (2005); Philos. Trans. R. Soc. London, Ser. A **364**, 601 (2006).
[7] S. V. Bulanov, F. Pegoraro, A. M. Pukhov, and A. S. Sakharov, Phys. Rev. Lett. **78**, 4205 (1997).
[8] L. M. Gorbunov, S. Yu. Kalmykov, and P. Mora, Phys. Plasmas **12**, 033101 (2005).
[9] A. G. Litvak, Sov. Phys. JETP **30**, 344 (1969); C. Max, J. Arons, and B. Langdon, Phys. Rev. Lett. **33**, 209 (1974); G.-Z. Sun, E. Ott, Y. C. Lee, and P. Guzdar, Phys. Fluids **30**, 526 (1987).
[10] P. Sprangle, E. Esarey, and A. Ting, Phys. Rev. Lett. **64**, 2011 (1990); Phys. Rev. A **41**, 4463 (1990).
[11] M. Uesaka, K. Kinoshita, T. Watanabe *et al.*, IEEE Trans. Plasma Sci. **PS-28**, 1133 (2000); D. Janssen, H. Büttig, P. Evtushenko *et al.*, Nucl. Instrum. Methods Phys. Res. A **507**, 314 (2003); I. V. Bazarov and C. K. Sinclair, Phys. Rev. ST Accel. Beams **8**, 034202 (2005).
[12] M. J. van der Wiel, O. J. Luiten, G. J. H. Brussaard, S. B. van der Geer, W. H. Urbanus, W. van Dijk, and Th. van Oudheusden, Philos. Trans. R. Soc. London, Ser. A **364**, 679 (2006).
[13] M. J. de Loos, S. B. van der Geer, Y. M. Saveliev *et al.*, Phys. Rev. ST Accel. Beams **9**, 084201 (2006).
[14] A. Doyuran, J. England, C. Joshi *et al.*, AIP Conf. Proc. **737**, 750 (2004).
[15] D. F. Gordon, R. F. Hubbard, J. H. Cooley, B. Hafizi, A. Ting, and P. Sprangle, Phys. Rev. E **71**, 026404 (2005).
[16] N. E. Andreev and S. V. Kuznetsov, Plasma Phys. Controlled Fusion **45**, A39 (2003).
[17] A. F. Lifschitz, J. Faure, V. Malka, and P. Mora, Phys. Plasmas **12**, 093104 (2005); A. F. Lifschitz, J. Faure, Y. Glinec, and V. Malka, Nucl. Instrum. Methods Phys. Res. A **561**, 314 (2006).
[18] N. E. Andreev, L. M. Gorbunov, V. I. Kirsanov, K. Nakajima, and A. Ogata, Phys. Plasmas **4**, 1145 (1997); G. Shvets and X. Li, *ibid.* **6**, 591 (1999).
[19] N. E. Andreev, L. M. Gorbunov, and R. R. Ramazashvili, Plasma Phys. Rep. **23**, 277 (1997).
[20] A. G. Khachatryan and S. S. Elbakian, Plasma Phys. Rep. **27**, 860 (2001).
[21] L. M. Gorbunov and V. I. Kirsanov, Sov. Phys. JETP **66**, 290 (1987); F. Dorchies, F. Amiranoff, V. Malka *et al.*, Phys. Plasmas **6**, 2903 (1999).
[22] A. G. Khachatryan, F. A. van Goor, K.-J. Boller, A. J. W. Reitsma, and D. A. Jaroszynski, Phys. Rev. ST Accel. Beams **7**, 121301 (2004).
[23] P. Chen, J. M. Dawson, R. W. Huff, and T. Katsouleas, Phys. Rev. Lett. **54**, 693 (1985).
[24] R. J. Noble, Phys. Rev. A **32**, 460 (1985).
[25] N. H. Matlis, S. Reed, S. S. Bulanov *et al.*, Nat. Phys. **2**, doi: 10.1038/nphys442 (2006).
[26] M. N. Rosenbluth and C. S. Liu, Phys. Rev. Lett. **29**, 701 (1972).
[27] L. M. Gorbunov, P. Mora, and T. M. Antonsen, Jr., Phys. Plasmas **4**, 4358 (1997).
[28] A. Solodov, Ph.D. thesis, École Polytechnique, Palaiseau, France, 2001, p. 25; available on-line at http://www.editions.polytechnique.fr/Theses/Files/Solodov200web.pdf
[29] P. Mora and T. M. Antonsen, Jr., Phys. Plasmas **4**, 217 (1997).
[30] P. Mora and F. Amiranoff, J. Appl. Phys. **66**, 3476 (1989); P. Mora, Phys. Fluids B **4**, 1630 (1992).
[31] E. Esarey and M. Pilloff, Phys. Plasmas **2**, 1432 (1995).
[32] N. E. Andreev, S. V. Kuznetsov, and I. V. Pogorelsky, Phys. Rev. ST Accel. Beams **3**, 021301 (2000).
[33] C. B. Schroeder, E. Esarey, B. A. Shadwick, and W. P. Leemans, Phys. Plasmas **13**, 033103 (2006).
[34] A. G. Khachatryan, Phys. Rev. E **65**, 046504 (2002).
[35] S. V. Bulanov, M. Yamagiwa, T. Zh. Esirkepov *et al.*, Phys. Plasmas **12**, 073103 (2005).
[36] T. Esirkepov, S. V. Bulanov, M. Yamagiwa, and T. Tajima, Phys. Rev. Lett. **96**, 014803 (2006).
[37] P. Mora, J. Appl. Phys. **71**, 2087 (1992).
[38] R. D. Ruth, A. W. Chao, P. L. Morton, and P. B. Wilson, Part. Accel. **17**, 171 (1985).
[39] A. J. W. Reitsma, V. V. Goloviznin, L. P. J. Kamp, and T. J. Schep, Phys. Rev. E **63**, 046502 (2001).
[40] S. Cheshkov, T. Tajima, W. Horton, and K. Yokoya, Phys. Rev. ST Accel. Beams **3**, 071301 (2000); C. Chiu, S. Cheshkov, and T. Tajima, *ibid.* **3**, 101301 (2000).
[41] I. Kostyukov, S. Kiselev, and A. Pukhov, Phys. Plasmas **10**, 4818 (2003); S. Kiselev, A. Pukhov, and I. Kostyukov, Phys. Rev. Lett. **93**, 135004

(2004); A. Rousse, K. Ta Phuoc, R. Shah *et al.*, *ibid.* **93**, 135005 (2004); K. Ta Phuoc, F. Burgy, J.-P. Rousseau *et al.*, Phys. Plasmas **12**, 023101 (2005); P. Michel, C. B. Schroeder, B. A. Shadwick, E. Esarey, and W. P. Leemans, Phys. Rev. E **74**, 026501 (2006).
[42]B. Quesnel and P. Mora, Phys. Rev. E **58**, 3719 (1998).
[43]R. Assmann and K. Yokoya, Nucl. Instrum. Methods Phys. Res. A **410**, 544 (1998).
[44]T. Plettner, R. L. Byer, E. Colby, B. Cowan, C. M. S. Sears, J. E. Spencer, and R. H. Siemann, Phys. Rev. ST Accel. Beams **8**, 121301 (2005); C. M. S. Sears, R. L. Byer, E. R. Colby, B. M. Cowan, R. Ischebeck, M. R. Lincoln, T. Plettner, R. H. Siemann, and J. E. Spencer, "Beam Coupling to Optical Scale Accelerator Structures," presented at the 12th Advanced Accelerator Concepts Workshop, Lake Geneva, Wisconsin, 2006 (to appear in AIP Conf. Proc.).
[45]D. A. Edwards and M. J. Syphers, *An Introduction to the Physics of High Energy Accelerators* (Wiley, New York, 1993), p. 252.
[46]D. Teychenné, G. Bonnaud, and J.-L. Bobin, Phys. Rev. E **48**, R3248 (1993).
[47]L. M. Gorbunov, P. Mora, and R. R. Ramazashvili, Phys. Rev. E **65**, 036401 (2002).
[48]I. S. Gradshteyn and I. M. Ryzhik, *Table of Integrals, Series and Products* (Academic, New York, 1980), pp. 232, 905.
[49]V. Malka, A. Lifschitz, J. Faure, and Y. Glinec, "Laser-Plasma Accelerators," presented at the 12th Advanced Accelerator Concepts Workshop, Lake Geneva, Wisconsin, 2006 (to appear in AIP Conf. Proc.).
[50]C. B. Schroeder, P. B. Lee, J. S. Wurtele, E. Esarey, and W. P. Leemans, Phys. Rev. E **59**, 6037 (1999); G. Fubiani, E. Esarey, C. B. Schroeder, and W. P. Leemans, *ibid.* **70**, 016402 (2004).
[51]S. P. D. Mangles, C. D. Murphy, Z. Najmudin *et al.*, Nature (London) **431**, 535 (2004); C. G. R. Geddes, Cs. Tóth, J. van Tilborg *et al.*, *ibid.* **431**, 538 (2004); J. Faure, Y. Glinec, A. Pukhov *et al.*, *ibid.* **431**, 541 (2004); S. P. D. Mangles, A. G. R. Thomas, M. C. Kaluza *et al.*, Phys. Rev. Lett. **96**, 215001 (2006).
[52]W. P. Leemans, B. Nagler, A. J. Gonsalves *et al.*, Nat. Phys. **2**, 696 (2006).